

Characterization of oncohistone H2B variants in *Schizosaccharomyces pombe* reveals a key role of H2B monoubiquitination deficiency in genomic instability by altering gene expression

Guangchun Lu[‡], Li Liu[‡], Mitchell Opoku, Ruifan Zhu, Haiyang Wang, Gang Feng[✉]

Jiangsu Key Laboratory for Pathogens and Ecosystems, College of Life Sciences, Nanjing Normal University, Nanjing 210023, China

*Corresponding author. College of Life Sciences, Nanjing Normal University, Nanjing 210023, China. E-mail: fengg@njnu.edu.cn

Editor: [John Morrissey]

[‡]These authors contributed equally to this work.

Abstract

Various amino acid substitutions commonly occur at one residue of a histone in human cancers, but it remains unclear whether these histone variants have distinct oncogenic effects and mechanisms. Our previous modeling study in the fission yeast *Schizosaccharomyces pombe* demonstrated that the oncohistone mutants H2BG52D, H2BD67N, and H2BP102L cause the homologous recombination defects and genomic instability by compromising H2B monoubiquitination (H2B^{ub}). However, it is unknown whether other amino acid changes at the H2B-Gly52/Asp67/Pro102 residues influence H2B^{ub} levels and whether they cause genomic instability by altering H2B^{ub}-regulated gene expression. Here, we construct diverse oncomutants at the sole H2B gene *htb1-Gly52/Asp67/Pro102* sites in *S. pombe* and study their impacts on genotoxic response, H2B^{ub} levels, and gene expression. Interestingly, the oncomutants *htb1-G52D*, *htb1-D67N*, and *htb1-P102L* exclusively exhibit significant genotoxic sensitivity, reduced H2B^{ub} levels, and altered gene expression. These defects can be rescued by restoring H2B^{ub} levels with the deletion of the H2B deubiquitinase *ubp8⁺*. These strong genetic correlations suggest that H2B^{ub} deficiency plays a determinant role in the genomic instability of *htb1-Gly52/Asp67/Pro102* oncomutants and that the alteration of gene expression due to reduced H2B^{ub} levels is a novel mechanism underlying the genomic instability caused by *htb1-G52D*, *htb1-D67N*, and *htb1-P102L* oncomutations.

Keywords: *Schizosaccharomyces pombe*; fission yeast; oncohistone H2B; H2B monoubiquitination; gene expression; genomic instability

Introduction

The missense mutations in a single copy of histone genes are frequently found in human cancers, and the encoded proteins are described as oncohistones (Mohammad and Helin 2017, Qiu et al. 2018). A residue of an oncohistone can be substituted for various amino acids with different frequencies (Funato and Tabar 2018). In the case of canonical oncohistones, H3K27M (lysine-to-methionine), H3G34R/V/W/L (glycine-to-arginine/valine/tryptophan/leucine), and H3K36M mutants occur most frequently in pediatric cancers (Liu et al. 2014, Kallappagoudar et al. 2015, Wan et al. 2018). Their common oncogenic mechanism is the perturbation of posttranslational modifications (PTMs) of histone H3 (Weinberg et al. 2017, Lowe et al. 2019, Espinoza Pereira et al. 2023). Two main consequences of perturbed histone PTMs are alteration in gene expression and genomic instability, both of which can promote oncogenesis (Dabin et al. 2024, Selvam et al. 2024, Yadav et al. 2024).

The H3K27M mutant, which occurs in 78% of diffuse intrinsic pontine gliomas, and the H3K27I (lysine-to-isoleucine) reduce the global H3K27me3 levels *in trans*, whereas the other 18 amino acid substitutions of H3K27 have no such effect (Lewis et al. 2013). However, the reduction in H3K27me3 levels and its impact on gene expression are not uniform across the genome (Chan et al.

2013). H3K27me3 abundance is reduced in weak PRC2 complex target genes and enhances their expression; however, H3K27me3 is retained in strong PRC2 target genes and silences genes (Sahu and Lu 2022). Therefore, the influence of H3K27M/I on gene expression in cancer may not be simply attributed to the loss of H3K27 methylation or PRC2 activity. In addition, H3K27M reduces homologous recombination (HR) and increases replication stress (Caeiro et al. 2024). The H3K36M mutant, which is identified in 95% of chondroblastomas, and the H3K36I both lead to reduced levels of global H3K36me2/3 and elevated levels of H3K27me2/3 *in trans*. However, other oncohistone H3K36R and nononcohistone H3K36L/A (lysine-to-leucine/alanine) have no such effects (Lu et al. 2016). The genome-wide altered gene expression does not appear to be determined mainly by the loss of H3K36me2/3. Instead, the gain and redistribution of H3K27me3 may play a more significant role in the gene expression profile of the H3K36M mutant (Sahu and Lu 2022). Moreover, H3K36M decreases the activity of HR repair for DNA breaks (Caeiro et al. 2024), and H3K36R is also defective in the response to DNA breaks (Zhang et al. 2023). Among the H3G34 oncomutants, the H3G34R/V are found in 20% of pediatric high-grade glioma, whereas H3G34W/L occur in 92% of giant cell tumors of the bone. These mutants decrease the abundance of H3K36me2/3 *in cis* (Chan et al. 2013,

Received 21 March 2025; revised 19 May 2025; accepted 20 May 2025

© The Author(s) 2025. Published by Oxford University Press on behalf of FEMS. This is an Open Access article distributed under the terms of the Creative Commons Attribution License (<https://creativecommons.org/licenses/by/4.0/>), which permits unrestricted reuse, distribution, and reproduction in any medium, provided the original work is properly cited.

Lewis et al. 2013, Fang et al. 2018, Shi et al. 2018). However, the aberrant gene expression in H3G34W can be restored by H3K27R (lysine-to-arginine), implying that the gain of H3K27me3 levels, rather than the loss of H3K36me3, could be its direct mechanism (Jain et al. 2020). Moreover, H3G34R attenuates HR and mismatch repair, and H3G34W compromises DNA repair via nonhomologous end joining (Caeiro et al. 2024). Collectively, the influences of canonical H3 oncohistones on gene expression and genome stability vary with different amino acid substitutions, which could not be attributed solely to changes in H3 PTMs.

In addition, many noncanonical oncomutants occur at both the tails and the globular domains of histones (Bennett et al. 2019). In contrast to the high frequency and tissue specificity of canonical H3 oncohistones in pediatric cancers, noncanonical histone oncomutants occur widely in ~4% of adult common tumors, and few are significantly associated with a particular type of tumor (Nacev et al. 2019). These noncanonical oncohistones affect chromatin states and remodeling (Mitchener and Muir 2022). However, the functional impacts and mechanisms of different amino acid substitutions at residues of noncanonical oncohistones remain largely unclear. A previous study showed that H3K9M rather than H3K9R (lysine-to-arginine) diminishes the overall amount of H3K9me2/3 (Lewis et al. 2013). In addition, both acetylation-deficient H4K91R and acetylation-mimic H4K91Q (lysine-to-glutamine) abolish the acetylation and ubiquitination of H4K91, resulting in genomic instability and abnormal development H4K91M mutation (Tessadori et al. 2017). Taken together, different amino acid substitutions in various noncanonical oncohistones could also exhibit distinct effects and mechanisms.

Therefore, comprehensive variant studies of a particular histone residue are required to gain mechanistic insights into the oncogenic effects of an oncohistone and determine whether it acts as a driver or passenger in cancer development. This poses a challenge to the aforementioned research conducted in mammalian cells, but can be readily achieved by modeling in yeast, which shares ~90% sequence identity with human H3/H4 and 70% identity with human H2A/H2B. In contrast to many copies of histone genes in humans, both budding and fission yeast contain only a few copies, which could amplify the oncomutant effects, facilitate genetic analysis by performing rapid and unbiased screens, and clarify the functional consequences of oncohistones (Shan et al. 2016, Yadav et al. 2017, Bagert et al. 2021, Lowe et al. 2021, Lemon et al. 2022, Zhang et al. 2023, Ohkuni et al. 2025, Sad et al. 2025). For instance, in a humanized budding yeast library, histone oncomutants are unbiasedly screened for their effects on chromatin remodeling (Bagert et al. 2021). In the fission yeast *Schizosaccharomyces pombe*, H3K9M traps histone methyltransferase Clr4 and blocks H3K9 methylation *in trans* (Shan et al. 2016). Another oncohistone, H3G34R, reduces H3K36me3 levels and leads to HR repair defect and genomic instability in *S. pombe* (Yadav et al. 2017). Although H3K36me3 levels are also reduced in H3G34V, H3G34R displays more severe genomic instability than H3G34V does, probably due to more H3K27 methylation and a distinct profile of gene expression in H3G34R. However, H3G34W and nononcohistones H3G34M/Q (glycine-to-methionine/glutamine) fail to decrease H3K36me3 levels and thus exhibit no defects in DNA damage repair and genome stability (Lowe et al. 2021). In the budding yeast *Saccharomyces cerevisiae*, H3G34R/V/W/L exhibit similar sensitivities to caffeine, formamide, and HU, whereas H3K36M/R are more sensitive to cellular stress, such as caffeine. This is linked to their reduced extent of H3K36me3 levels (Lemon et al. 2022). Another study demonstrated that H3E50K/R (glutamic acid-to-lysine/arginine) confer

greater sensitivities to caffeine and bleomycin than H3E50A (glutamic acid-to-alanine) does in *S. cerevisiae*, but they cause similar reductions in certain H3 N-tail PTMs (Sad et al. 2025). Moreover, the highly frequent H3E97K and uncommon H3E97A exhibit similar chromosomal instability by reducing the interaction with H4 and facilitating CENP-A mislocalization in *S. cerevisiae* (Ohkuni et al. 2025). In addition to oncohistone H3, yeast is also emerging as an excellent model for studying oncohistone H2B (Wan and Chan 2021). H2BE76K is the most frequent H2B oncomutant, and its conserved H2BE79K in *S. cerevisiae* is more sensitive to a high temperature than H2BE79Q (glutamic acid-to-glutamine), possibly because H2BE79K renders the nucleosome more unstable than H2BE79Q (Bennett et al. 2019).

Our previous study characterized the conserved and common H2B oncohistone mutants in *S. pombe*, whose genome contains a single histone H2B-encoding gene compared with two genes in *S. cerevisiae* and 23 genes in humans (Zhang et al. 2023). We revealed that H2BE112K and H2BE34K mutants have more severe genotoxic defects than those of H2BE112Q and H2BE34D, respectively. Importantly, H2BG52D (glycine-to-aspartic acid), H2BD67N (aspartic acid-to-asparagine), and H2BP102L (proline-to-leucine) reduce the levels of H2B monoubiquitination at Lys119 (H2B^{ub}), leading to oncogenic phenotypes such as genomic instability by compromising the ability of HR repair (Qin et al. 2024). In addition to regulating HR, H2B^{ub} also modulates gene expression. Therefore, it remains unclear whether other amino acid substitutions at the H2B-Gly52/Asp67/Pro102 sites reduce H2B^{ub} levels and whether they cause genomic instability by altering gene expression. In this study, we constructed various oncomutants at a single site of the H2B gene *htb1-Gly52/Asp67/Pro102* in *S. pombe* and investigated their effects on genotoxic response, H2B^{ub} levels, and gene expression. Furthermore, we studied the effects of H2B^{ub} restoration on gene expression in *htb1-G52D*, *htb1-D67N*, and *htb1-P102L* oncomutants. Interestingly, among the various *htb1-Gly52/Asp67/Pro102* mutants, *htb1-G52D*, *htb1-D67N*, and *htb1-P102L* exclusively displayed significant genotoxic sensitivity, reduced H2B^{ub} levels, and altered gene expression. These effects were restored to normal levels after rescuing H2B^{ub} levels with the deletion of the H2B deubiquitinase *ubp8⁺*.

Materials and methods

Schizosaccharomyces pombe strains, plasmids, and antibodies

Schizosaccharomyces pombe strains were constructed by standard Polymerase Chain Reaction (PCR)-based transformation or mating (Bähler et al. 1998, Forsburg and Rhind 2006, Sabatinos and Forsburg 2010). Briefly, the DNA fragment containing 5' UTR and upstream sequences (422 bp), CDS (381 bp), and 3' UTR (639 bp) of the *htb1⁺* gene was PCR amplified from *S. pombe* genomic DNA as 5' overhang. The fragment of 3' UTR downstream sequence (343 bp) of *htb1⁺* was also PCR amplified as 3' overhang. The 5' overhang of *htb1⁺* was cloned into the upstream of *kanMX6* at the *Bam*HI and *Bgl*II sites of the pFA6a-*kanMX6* plasmid, and the 3' overhang of *htb1⁺* was cloned into the downstream of *kanMX6* at the *Sac*I and *Sac*II sites of pFA6a-*kanMX6*. The resulting plasmid was named as pGF2. Various *htb1-Gly52/Asp67/Pro102* (the number of an H2B residue in *S. pombe* is one less than that in humans) mutations in pGF2 were generated by site-directed mutagenesis. The 5' overhang fragment with *htb1-Gly52/Asp67/Pro102* mutations, *kanMX6*, and the 3' overhang of *htb1⁺* were then PCR amplified to form the full fragment (3231 bp), which was

transformed to *S. pombe* cells. The G418 resistant colonies were verified by colony PCR and sequenced for various *htb1-Gly52/Asp67/Pro102* mutations. The strain genotypes are listed in Table S1. The information on the plasmids is presented in Table S2. The use of antibodies is shown in Table S3.

Spot assay of *S. pombe* growth

The spot assay was performed according to our previous publications (Feng et al. 2019, Qin et al. 2024, Lu et al. 2025). *Schizosaccharomyces pombe* cells were grown to the log phase, adjusted to an optical density (OD₆₀₀) of 0.5, and serially 5-fold diluted. Each dilution was spotted onto plates containing the indicated genotoxic drugs at 30°C. The drugs used are hydroxyurea (HU) (Sigma, H8627, St. Louis, MO, USA), camptothecin (CPT) (Sigma, C9911), methyl methanesulfonate (MMS) (Sigma, 129925), phleomycin (Phleo) (MCE, HY-126490, Monmouth Junction, NJ, USA), bleomycin (Bleo) (MCE, HY-17565), and 6-azauracil (6-AU) (Sigma, A1757). The plates were incubated for the indicated days and photographed.

Protein extraction and immunoblotting

Whole-cell protein extraction and immunoblotting were based on our previous methods (Feng et al. 2019, Qin et al. 2024, Lu et al. 2025). The log phase *S. pombe* cells with 10 ml at OD₆₀₀ = 1.0 were incubated in lysis buffer (0.9 M NaOH and 3.5% 2-mercaptoethanol) and then added with an equal volume of 55% trichloroacetic acid (Sigma, 91228). The cells were then centrifuged and resuspended in 2x protein SDS-loading buffer. After neutralization with 1 M Tris, the cells were boiled at 90°C for 5 min. The proteins were subsequently subjected to SDS-PAGE, transferred, and detected with an Odyssey infrared imaging system (Li-COR) (Lincoln, NE, USA). After exposure, the blots containing whole-cell proteins were stained with Coomassie Brilliant Blue (CBB), which served as an independent loading control of total proteins. The quantitation of the abundance of H2B^{ub} or FLAG-tagged protein is normalized to total protein levels measured by CBB staining (Leng et al. 2022).

RNA-seq analysis of the transcriptome

RNA-seq was performed based on our previous studies (Qin et al. 2024, Lu et al. 2025). Total RNA for RNA-seq was extracted with a Trizol Kit (Invitrogen, Carlsbad, CA, USA) and mRNA was enriched with oligo(dT) beads. Following fragmentation, cDNA was synthesized, ligated, and amplified via PCR. The PCR products were sequenced with an Illumina HiSeq 2500 instrument by Gene Denovo Biotechnology. The raw reads were filtered and removed from rRNA. Clean reads were mapped to the *S. pombe* reference genome (Ensembl_release45) using HISAT2. The read count was transformed to the fragment per kilobase of transcript per million mapped reads value as a measure of gene expression levels via StringTie. The differentially expressed genes (DEGs) were defined as transcripts with false discovery rate or *q* value below 0.05 and more than 2-fold change in expression. The data were averaged from three independent biological repeats and analyzed with the Omicsmart online platform (<http://www.omicsmart.com>). The expression of all genes in the indicated strains is listed in Tables S5–S7. A list of DEGs in the indicated strains is included in Tables S8–S10.

RNA extraction

Total RNA was prepared as described previously with some modifications (Feng et al. 2013). Briefly, 50 ml of cells at OD₆₀₀ = 1.0

were harvested and resuspended in 750 µl of lysis buffer (50 mM NaOAc, 10 mM EDTA, and 1% SDS). The resuspended cells were combined with 750 µl of acid phenol (pH 4.7) (Ambion, Austin, TX, USA) and incubated at 65°C for 1 h with shaking. The cell lysates were cooled and centrifuged for 5 min at 20 000 × *g*. The aqueous phase was extracted with phenol–chloroform (pH 7.5) repeatedly until the interfaces were no longer white. After the addition of 3 M NaOAc and 100% ethanol, the RNA was precipitated and stored at –80°C until use.

Reverse transcription and quantitative PCR

The reverse transcription and quantitative PCR (RT-qPCR) assay was conducted and analyzed as described in our previous publication (Feng et al. 2013). Total RNA (200 ng µl⁻¹) was treated with gDNA Wiper Mix (Vazyme, R323, Nanjing, Jiangsu, China) at 42°C for 2 min to remove any contaminated genomic DNA. Then, 500 ng of total RNA was reverse transcribed into cDNA using random primers with the HiScript III qRT Super Mix (Vazyme, R323). After cDNA was synthesized and diluted to ~10 ng ml⁻¹, 6 µl of this cDNA template, 10 µl of 2x SYBR Green qPCR master mix (Vazyme, Q712), and 4 µl of primer sets for the indicated genes were mixed and run on an ABI QuantStudio Real-Time PCR instrument (Carlsbad, CA, USA). The expression of the genes was determined by the comparative Ct (2^{-Ct}) method and normalized to that of *act1*⁺, whose expression remained unchanged under the indicated experimental conditions in RNA-seq and immunoblotting assays. We further normalized the gene expression in the indicated mutants to that in the wild-type (WT) (arbitrarily set as 1) as the relative fold change, which was averaged from three independent biological repeats. The RT-qPCR primers used are listed in Table S4.

Chromatin immunoprecipitation and quantitative PCR

The chromatin immunoprecipitation and quantitative PCR (ChIP-qPCR) assay was performed as previously described (Feng et al. 2019, Qin et al. 2024). To prevent H2B^{ub} from deubiquitination, *S. pombe* cells grown in YES media were treated with 20 mM of the fresh deubiquitinase inhibitor *N*-ethylmaleimide (NEM) (Sigma, E1271) for 30 min before cross-linking. The cells with 100 ml at OD₆₀₀ = 1.0 were then cross-linked with 1% formaldehyde (Sigma, 47608) at 25°C for 20 min and neutralized by adding a 1/20 volume of 2.5 M glycine. The cells were subsequently resuspended in lysis buffer [50 mM HEPES, pH 7.2; 150 mM NaCl; 1 mM EDTA; 1% Triton X-100; 0.1% sodium deoxycholate (SDC)] supplemented with 1x yeast protease inhibitors (Sangon, C510026, Shanghai, China) and/or 20 mM of fresh NEM. The cells were then bead-beaten with FastPrep (MP Biomedicals, CA, USA). After centrifugation, the supernatant was sonicated to an average of 500 bp of DNA fragments as input. The chromatin samples were incubated with the indicated antibodies and then incubated with protein A/G agarose beads (Thermo, 26 159, Waltham, MA, USA). After washing with lysis buffer, high-salt buffer (50 mM HEPES, pH 7.2; 500 mM NaCl; 1 mM EDTA; 1% Triton X-100; 0.1% SDC), and LiCl buffer (20 mM Tris, pH 8.0; 250 mM LiCl; 0.5% NP-40; 0.5% SDC), the immunoprecipitated chromatin was eluted and reverse cross-linked with 1% SDS at 65°C overnight. The immunoprecipitated and input DNA were digested with 100 µg ml⁻¹ proteinase K (NEB, P8102, Ipswich, MA, USA) and 100 µg ml⁻¹ RNase A (Thermo, EN0531, Waltham, MA, USA) and purified with the MinElute PCR purification kit (Qiagen, 28004, Düsseldorf, Germany). 6 µl of diluted DNA template, 10 µl of 2x SYBR Green PCR master mix (Vazyme, Q712), and 4 µl

of the indicated primers (Table S4) were mixed and run on an ABI QuantStudio Real-Time PCR instrument. The enrichment was calculated as the percentage of immunoprecipitated DNA relative to the input DNA levels by the comparative Ct (2^{-Ct}) method. We normalized the enrichment in the H2B oncomutants to that in the WT (set as 1) as the relative fold change at the indicated locus.

Structural prediction of nucleosomes with oncohistones

Structural predictions of *S. pombe* nucleosomes with oncohistones were conducted via the AlphaFold 3 server (<https://www.alphafoldserver.com>) with default parameters (Jumper et al. 2021, Abramson et al. 2024). The structures were visualized via PyMOL software.

Statistical analysis

Statistical analysis was conducted using GraphPad Prism software (San Diego, CA, USA). All the data are expressed as the means with error bars indicating standard deviations (SDs) from two or three independent biological repeats. ns, *, **, ***, and **** indicate no significance, $P < .05$, $P < .01$, $P < .001$, and $P < .0001$, respectively.

Results

The diverse *htb1*-Gly52 oncomutants exhibit distinct temperature and genotoxic phenotypes

In a previous study, we modeled H2B oncohistones by mutating their single gene *htb1*⁺ and expressing each variant as the sole copy of histone H2B in *S. pombe*. We found that the *htb1*-G52D, *htb1*-D67N, and *htb1*-P102L oncomutations cause the HR repair defect and genomic instability by reducing H2B^{ub} levels (Qin et al. 2024). To test whether other amino acid substitutions at the H2B-Gly52 residue have similar effects on genome maintenance, we created four other different missense oncomutants at the same H2B-Gly52 residue in *S. pombe*. These mutants were ranked by their mutation frequencies in human tumors as follows: *htb1*-G52D (glycine-to-aspartic acid) > *htb1*-G52C (glycine-to-cysteine) > *htb1*-G52R (glycine-to-arginine) > *htb1*-G52S (glycine-to-serine) > *htb1*-G52A (glycine-to-alanine) (Bennett et al. 2019, Nacev et al. 2019). Additionally, we introduced a negatively charged Glu to generate the nononcohistone *htb1*-G52E, which is similar to *htb1*-G52D but has not been reported in tumors. We subsequently evaluated their growth by spotting two independent repeats of strains onto plates under the following conditions: optimal temperature (30°C); high temperature (36°C); replication stress (HU, MMS, and CPT); DNA damage (bleomycin, phleomycin, and UV irradiation); and transcription elongation inhibitor (6-AU). Among the *htb1*-Gly52 mutants, only *htb1*-G52D exhibited slightly slower growth compared with WT and other *htb1*-Gly52 mutants at 30°C. Moreover, *htb1*-G52D was temperature-sensitive at 36°C, whereas *htb1*-G52E exhibited mild sensitivity (Fig. 1A and Fig. S1A). Interestingly, all the mutants except *htb1*-G52A showed varying degrees of sensitivity to at least one genotoxic agent (Fig. 1A and Fig. S1A). This implies that these five H2B mutants (*htb1*-G52D, *htb1*-G52C, *htb1*-G52R, *htb1*-G52S, and *htb1*-G52E) possibly exhibit DNA damage repair defects and genomic instability. In particular, the *htb1*-G52D mutant showed the most severe sensitivity, whereas the *htb1*-G52E and *htb1*-G52S showed less sensitivity than that of *htb1*-G52D. The genotoxic sensitivities of *htb1*-G52C and *htb1*-G52R were significantly lower compared with those of *htb1*-

G52D, *htb1*-G52E, and *htb1*-G52S (Fig. 1A and Fig. S1A). When exposed to 6-AU, the *htb1*-G52D exhibited little sensitivity, while *htb1*-G52E displayed sensitivity (Fig. 1A and Fig. S1A). As *htb1*-G52D or its analogue *htb1*-G52E possibly reduces H2B^{ub} levels (Qin et al. 2024), this 6-AU finding is consistent with a key role of H2B^{ub} in transcription regulation and suggests that the other four *htb1*-Gly52 mutants potentially have no effects on H2B^{ub} levels.

Only *htb1*-D67N among the *htb1*-Asp67 diverse oncomutants is sensitive to high temperature and DNA damage

In addition, we constructed three *htb1*-Asp67 oncomutants and ranked them according to their frequencies in human tumors as follows: *htb1*-D67N > *htb1*-D67H (aspartic acid-to-histidine) > *htb1*-D67G (aspartic acid-to-glycine). The nononcohistone *htb1*-D67A (aspartic acid-to-alanine) was also generated as an expected negative control. Moreover, Gln was incorporated to generate the *htb1*-D67Q (aspartic acid-to-glutamine) mutant, which shares similar amino acid properties with *htb1*-D67N. We then investigated the effects of high temperature, DNA damage, and replication stress on their growth. We observed that only *htb1*-D67N showed a growth defect at the optimal temperature of 30°C and displayed a more severe defect at 36°C (Fig. 1B and Fig. S1B). Surprisingly, only the *htb1*-D67N exhibited sensitivities to replication stress (HU, MMS, and CPT treatments) and DNA damage (bleomycin, phleomycin, and UV irradiation) (Fig. 1B and Fig. S1B). As expected, the *htb1*-D67N, which reduces H2B^{ub} levels (Qin et al. 2024), showed strong sensitivity in the presence of 6-AU treatment (Fig. 1B and Fig. S1B), suggesting that the other four *htb1*-Asp67 mutants potentially display no defect in H2B^{ub} levels.

Only *htb1*-P102L among the *htb1*-Pro102 diverse oncomutants shows the sensitivities to high temperature and genotoxins

Moreover, we constructed three different *htb1*-Pro102 oncomutants and ranked them by mutation frequency as follows: *htb1*-P102S (proline-to-serine) > *htb1*-P102L > *htb1*-P102T (proline-to-threonine). The *htb1*-P102A (proline-to-alanine) was created as a nononcohistone control, and Ile was used to generate the *htb1*-P102I (proline-to-isoleucine), which resembles *htb1*-P102L. We observed that all the *htb1*-Pro102 mutants were not defective in growth at optimal temperature (30°C). Interestingly, only the *htb1*-P102L grew much more slowly at 36°C (Fig. 1C and Fig. S1C). Similarly, only the *htb1*-P102L exhibited the great sensitivity to MMS and CPT but not HU, and the mild sensitivity to DNA damage (bleomycin, phleomycin, and UV irradiation). The other four *htb1*-Pro102 mutants showed no such sensitivities (Fig. 1C and Fig. S1C). In the case of 6-AU, only the *htb1*-P102L, which reduces H2B^{ub} levels (Qin et al. 2024), exhibited sensitivity (Fig. 1C and Fig. S1C), suggesting that the other four *htb1*-Pro102 mutants do not potentially affect H2B^{ub} levels.

The *htb1*-G52D, *htb1*-D67N, and *htb1*-P102L among the *htb1*-Gly52/Asp67/Pro102 diverse oncomutants decrease H2B^{ub} levels

To investigate the effects of diverse *htb1*-Gly52/Asp67/Pro102 mutants on H2B^{ub} levels, we performed an immunoblotting assay to measure H2B^{ub} levels. The *htb1*-K119R mutant served as a control for the absence of H2B^{ub}. Among the six *htb1*-Gly52 mutants, the H2B^{ub} levels were significantly decreased in

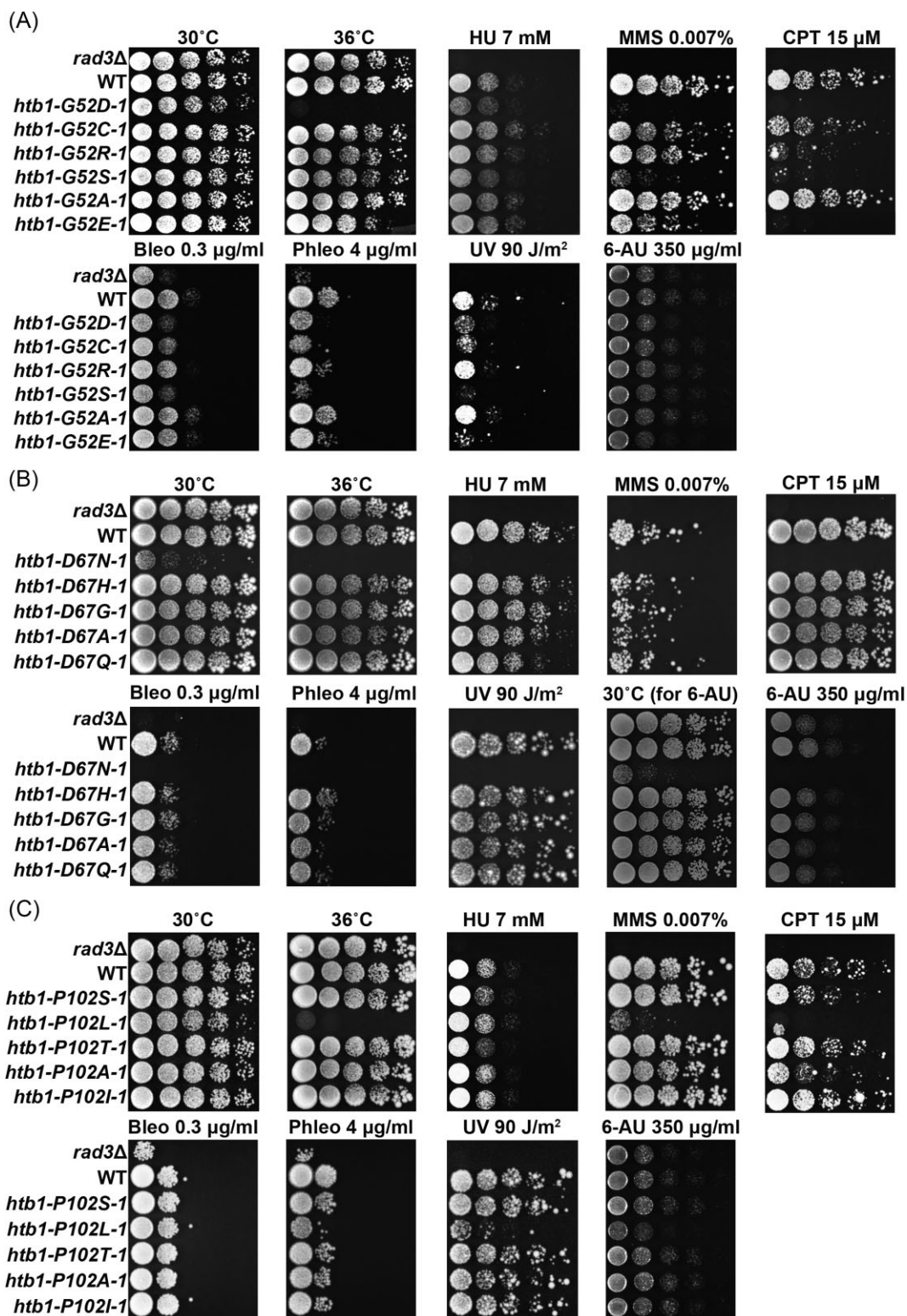


Figure 1. The temperature and genotoxic phenotypes of the *htb1*-Gly52/Asp67/Pro102 diverse mutants. (A) The growth of WT (TK8), *htb1*-G52D (YGF277), *htb1*-G52C (YGF507), *htb1*-G52R (YGF510), *htb1*-G52S (YGF460), *htb1*-G52A (YGF459), and *htb1*-G52E (YGF508) strains under indicated conditions. (B) The growth of WT (TK8), *htb1*-D67N (YGF324), *htb1*-D67H (YGF515), *htb1*-D67G (YGF514), *htb1*-D67A (YGF513), and *htb1*-D67Q (YGF509) strains under indicated conditions. (C) The growth of WT (TK8), *htb1*-P102S (YGF325), *htb1*-P102L (YGF279), *htb1*-P102T (YGF512), *htb1*-P102A (YGF511), and *htb1*-P102I (YGF505) strains under the indicated conditions. The *rad3Δ* (LD297) strain is a positive control. The length of incubation time is 4 days.

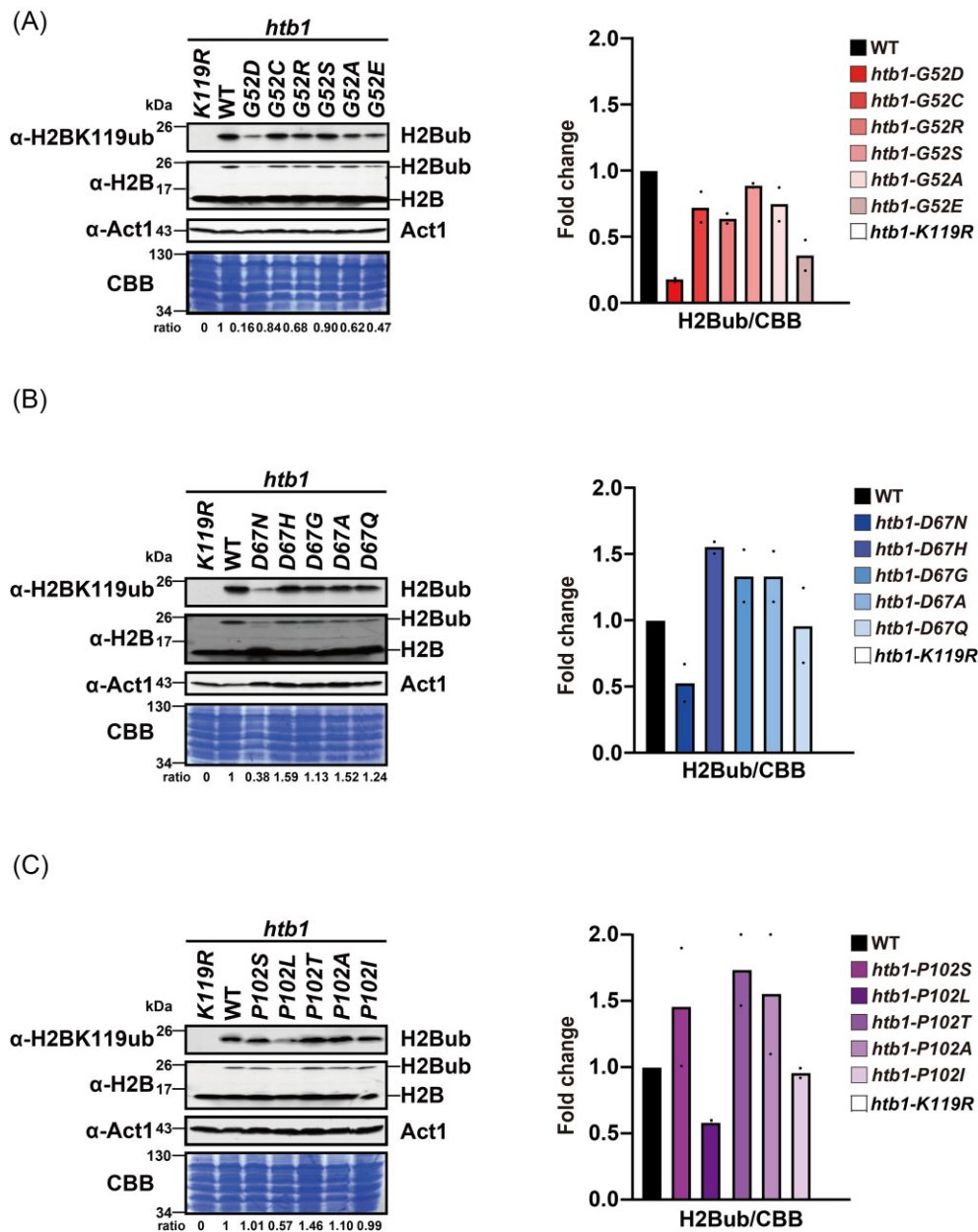


Figure 2. The levels of H2B^{ub} in the *htb1*-Gly52/Asp67/Pro102 diverse mutants. (A) Immunoblots of H2B^{ub} levels in *htb1*-K119R (YGF226), WT (TK8), *htb1*-G52D (YGF277), *htb1*-G52C (YGF507), *htb1*-G52R (YGF510), *htb1*-G52S (YGF460), *htb1*-G52A (YGF459), and *htb1*-G52E (YGF508) cells. (B) Immunoblots of H2B^{ub} amounts in *htb1*-K119R (YGF226), WT (TK8), *htb1*-D67N (YGF324), *htb1*-D67H (YGF515), *htb1*-D67G (YGF514), *htb1*-D67A (YGF513), and *htb1*-D67Q (YGF509) cells. (C) Immunoblots of H2B^{ub} abundance in *htb1*-K119R (YGF226), WT (TK8), *htb1*-P102S (YGF325), *htb1*-P102L (YGF279), *htb1*-P102T (YGF512), *htb1*-P102A (YGF511), and *htb1*-P102I (YGF505) cells. Left panel: the representative immunoblots from a biological replicate are shown. The intensity of the H2B^{ub} band is normalized to that of CBB staining. The fold change of this normalization factor in the indicated mutants relative to WT (set as 1) is denoted as the ratio at the bottom. Right panel: quantification of the relative fold change is plotted. Data represent the mean with minimum and maximum values from two independent biological replicates.

htb1-G52D and *htb1*-G52E cells (Fig. 2A and Fig. S2A). We also found that the H2B^{ub} levels in *htb1*-D67N alone were reduced among the five *htb1*-Asp67 mutants (Fig. 2B and Fig. S2B). Moreover, only *htb1*-P102L expressed lower levels of H2B^{ub} compared with the other four *htb1*-Pro102 mutants (Fig. 2C and Fig. S2C). The levels of H2B were fairly similar among these H2B variants. Collectively, the certain *htb1*-Gly52/Asp67/Pro102 mutants with decreased H2B^{ub} levels also show genotoxic sensitivity. This strong correlation indicates that H2B^{ub} plays a crucial role in the response of *htb1*-Gly52/Asp67/Pro102 oncomutants to DNA damage.

The *htb1*-G52D, *htb1*-D67N, and *htb1*-P102L among *htb1*-Gly52/Asp67/Pro102 diverse oncomutants alter genome-wide gene expression

Our previous finding showed that a reduction in H2B^{ub} levels impairs Rad51 recruitment for HR repair in *htb1*-G52D and *htb1*-P102L cells (Qin et al. 2024). In addition to its role in DNA repair, H2B^{ub} plays a key role in regulating transcription (Xiao et al. 2005, Tanny et al. 2007, Fuchs and Oren 2014, Chen et al. 2022). We thus hypothesized that the reduction in H2B^{ub} levels could lead to DNA repair defects in *htb1*-Gly52/Asp67/Pro102

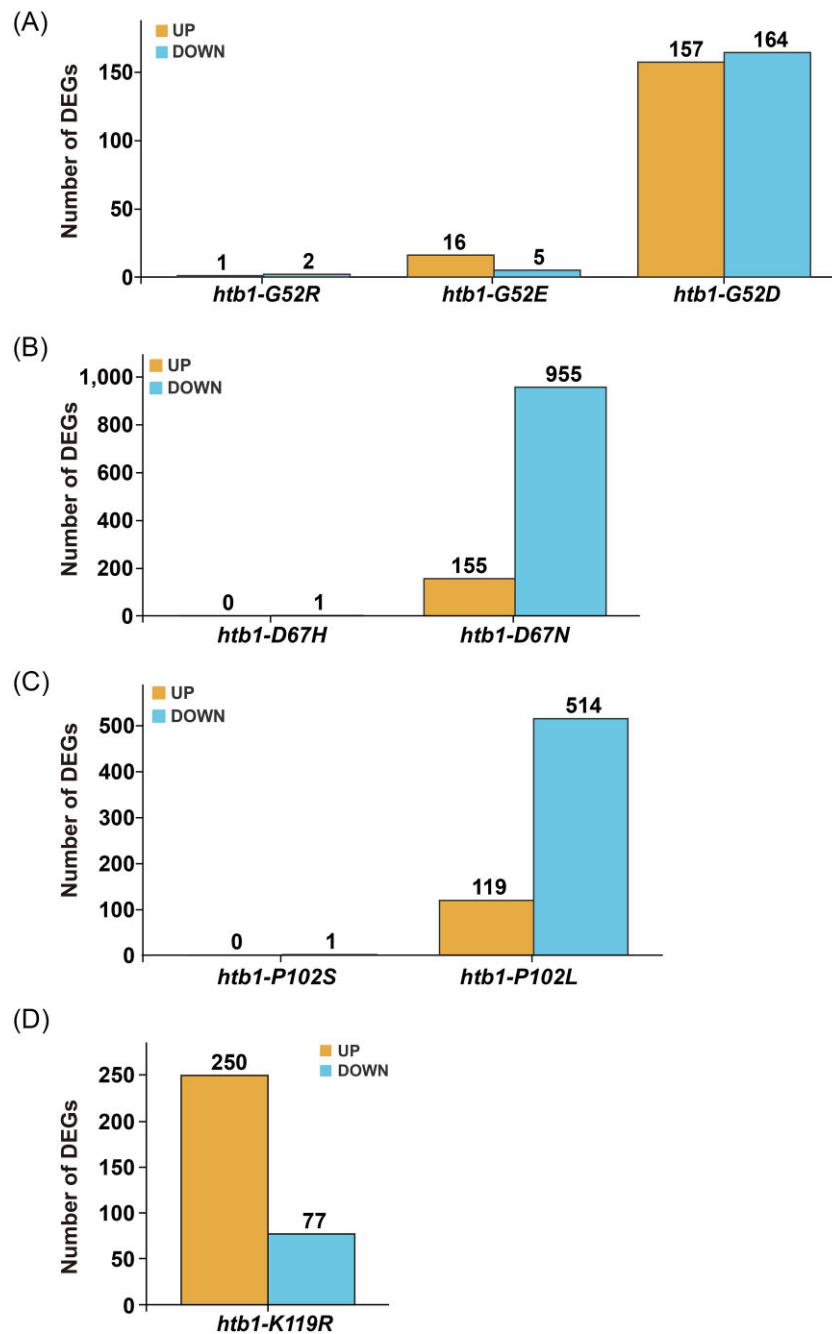


Figure 3. RNA-seq analysis of gene expression in the indicated *htb1*-Gly52/Asp67/Pro102 oncomutants. (A) RNA-seq analysis of DEGs relative to WT cells in *htb1-G52D* (YGF277), *htb1-G52R* (YGF510), and *htb1-G52E* (YGF508). (B) RNA-seq analysis of DEGs relative to WT cells in *htb1-D67N* (YGF324) and *htb1-D67H* (YGF515). (C) RNA-seq analysis of DEGs relative to WT cells in *htb1-P102S* (YGF325) and *htb1-P102L* (YGF279). (D) RNA-seq analysis of DEGs relative to WT cells in *htb1-K119R* (YGF226). The number of genes with up- and downregulated expression is indicated at the top of the column.

mutants by affecting the transcriptome. To test this hypothesis, we conducted an RNA-seq experiment and analyzed the transcriptomes of *htb1-G52D/E/R*, *htb1-D67N/H*, and *htb1-P102L/S* as a proof-of-principle. We found that the expression of 157 genes was significantly upregulated and 164 genes were downregulated in *htb1-G52D*, whereas the expression of few genes was altered in *htb1-G52E/R* (Fig. 3A and Table S8). Moreover, the expression of 155 genes was elevated, and the expression of 955 genes was reduced in *htb1-D67N*. In contrast, the expression of only one

gene was altered in *htb1-D67H* (Fig. 3B and Table S8). In the case of *htb1-P102L*, the expression of 119 genes was increased, and the expression of 514 genes was decreased, whereas the expression of only one gene was decreased in *htb1-P102S* (Fig. 3C and Table S8). Moreover, the Venn Diagram demonstrated the remarkable difference in up- and downregulated genes in *htb1-G52D* (Fig. S3A), *htb1-D67N* (Fig. S3B), and *htb1-P102L* (Fig. S3C), compared with *htb1-G52E/R*, *htb1-D67H*, and *htb1-P102S*, respectively. Gene ontology (GO) analysis also revealed different numbers and

classifications of altered genes in *htb1-G52D* (Fig. S3D), *htb1-D67N* (Fig. S3E), and *htb1-P102L* (Fig. S3F). To further test whether altered gene expression in *htb1-G52D/D67N/P102L* is associated with H2B^{ub} levels, we performed RNA-seq in *htb1-K119R* and found that the expression of 250 genes was significantly increased and that the expression of 77 genes was decreased (Fig. 3D and Table S9). We noticed that there were a significant number of overlapping genes with up- and downregulated expression between *htb1-K119R* and *htb1-G52D* (Fig. S3G), *htb1-D67N* (Fig. S3H), and *htb1-P102L* (Fig. S3I). We also observed similar GO patterns of altered genes between *htb1-K119R* and *htb1-G52D/D67N/P102L* (Fig. S3J). These results suggest that altered gene expression in *htb1-G52D/D67N/P102L* correlates with the genes regulated by H2B^{ub}.

The downregulated transcripts and proteins in *htb1-G52D*, *htb1-D67N*, and *htb1-P102L* are correlated with reduced H2B^{ub} levels

We previously found that the expression of DNA repair genes was not generally affected in *htb1-G52D/D67N/P102L* (Qin et al. 2024). Thus, to further validate that H2B^{ub} is involved in gene dysregulation in *htb1-G52D/D67N/P102L*, we focused on the expression of four representative genes: *aat1+*, *eng1+*, *ppk1+*, and *SPBC887.17+*, whose transcript levels were downregulated in *htb1-K119R* according to previous microarray data (Tanny et al. 2007) and our RNA-seq data (Fig. 3D and Table S9). The *aat1+* gene encodes an amino acid transmembrane transporter in the plasma membrane. The *eng1+* gene produces an endoglucanase involved in cell wall catabolism. The *ppk1+* gene encodes the serine/threonine protein kinase Ppk1, and its *S. cerevisiae* homolog Kin4 is a spindle position checkpoint and mitosis regulator (D'Aquino et al. 2005, Pereira and Schiebel 2005, Ekal et al. 2023). The *SPBC887.17+* gene is inferred to encode a guanine and adenine transmembrane transporter in the plasma membrane. We performed RT-qPCR experiments and validated that the levels of their transcripts were indeed decreased in *htb1-K119R* (Fig. 4A). We also found that their transcript levels were increased in *ubp8Δ*, which is a null mutant of H2B deubiquitinase *ubp8+* (Fig. 4A). The RNA levels of *aro1+* gene, which is independent of H2B^{ub} regulation and used as a negative control (Tanny et al. 2007), were consistently unaltered in our *htb1-K119R* and *ubp8Δ* mutants (Fig. S4A). These data suggest that transcription of these four genes is regulated by H2B^{ub}. Subsequently, we used RT-qPCR to verify the RNA levels of these four genes in certain *htb1-Gly52/Asp67/Pro102* mutants that were subjected to RNA-seq. We found that the levels of *aat1+*, *eng1+*, *ppk1+*, and *SPBC887.17+* transcripts were reduced in *htb1-G52D*, *htb1-D67N*, and *htb1-P102L* but not in *htb1-G52R/G52E*, *htb1-D67H*, and *htb1-P102S* (Fig. 4B). The RNA levels of the control gene *aro1+* were unaltered in these mutants (Fig. S4B). Additionally, we determined the RNA levels of *aat1+* and *ppk1+* in all the constructed *htb1-Gly52/Asp67/Pro102* mutants. Consistent with the results of H2B^{ub} levels, *htb1-G52D* (Fig. 4C), *htb1-D67N* (Fig. 4D), and *htb1-P102L* (Fig. 4E) exclusively exhibited reduced RNA levels of *aat1+* and *ppk1+*. To verify these results, we tagged *aat1+*, *eng1+*, and *ppk1+* with 5x FLAG at their C-termini and performed immunoblotting to examine whether their protein levels were correlated with their transcript levels. Consistently, the abundance of the Aat1-5FLAG (Fig. 4F), Eng1-5FLAG (Fig. 4G), and Ppk1-5FLAG (Fig. 4H) proteins were decreased in *htb1-G52D*, *htb1-P102L*, and more significantly reduced in *htb1-K119R*. Taken together, the correlations in these representative RNA and protein levels between *htb1-K119R* and *htb1-G52D/D67N/P102L* suggest that gene dysreg-

ulation in *htb1-G52D/D67N/P102L* mutants is the consequence of compromised H2B^{ub} levels.

The dysregulation of transcripts in *htb1-G52D*, *htb1-D67N*, and *htb1-P102L* is restored by the absence of *ubp8+*

To further support that H2B^{ub} deficiency in *htb1-G52D*, *htb1-D67N*, and *htb1-P102L* is the main mechanism for the dysregulation of their transcripts, we performed RNA-seq experiments in our previously constructed strains *htb1-G52D ubp8Δ*, *htb1-D67N ubp8Δ*, and *htb1-P102L ubp8Δ*, where deletion of *ubp8+* restored H2B^{ub} levels (Qin et al. 2024). Interestingly, the number of altered transcripts, particularly for the reduced transcripts, in *htb1-G52D ubp8Δ* (Fig. 5A and Table S10), *htb1-D67N ubp8Δ* (Fig. 5B and Table S10), and *htb1-P102L ubp8Δ* (Fig. 5C and Table S10) was significantly lower than that in *htb1-G52D*, *htb1-D67N*, and *htb1-P102L*, respectively. The Venn Diagram also showed no significant overlap for the downregulated genes in *htb1-G52D ubp8Δ* (Fig. 5D), *htb1-D67N ubp8Δ* (Fig. 5E), and *htb1-P102L ubp8Δ* (Fig. 5F) compared with *htb1-G52D*, *htb1-D67N*, and *htb1-P102L*, respectively. Despite there being a significant overlap for the upregulated and dysregulated genes, the number of overlapping genes was much smaller in *htb1-G52D* (Fig. S5A), *htb1-D67N* (Fig. S5B), and *htb1-P102L* (Fig. S5C). Moreover, GO analysis revealed a significant difference in the number and classification of affected genes in *htb1-G52D ubp8Δ* (Fig. S5D), *htb1-D67N ubp8Δ* (Fig. S5E), and *htb1-P102L ubp8Δ* (Fig. S5F). To validate these RNA-seq data, we measured the levels of *aat1+*, *eng1+*, *ppk1+*, and *SPBC887.17+* transcripts in *htb1-G52D*, *htb1-D67N*, and *htb1-P102L* with and without *ubp8+* by RT-qPCR. Consistent with the result shown in Fig. 4(B), the levels of *aat1+*, *eng1+*, *ppk1+*, and *SPBC887.17+* transcripts were reduced in *htb1-G52D*, *htb1-D67N*, and *htb1-P102L*. After deleting *ubp8+*, the levels of these transcripts were almost restored to WT levels (Fig. 5G). Collectively, these data indicate that the altered levels of transcripts in *htb1-G52D*, *htb1-D67N*, and *htb1-P102L* are mechanistically due to H2B^{ub} deficiency.

The downregulated transcripts in *htb1-G52D*, *htb1-D67N*, and *htb1-P102L* are caused by the reduced H2B^{ub} levels and the defect in RNA polymerase II elongation

To test whether H2B^{ub} levels are diminished at these representative genes whose expression is decreased in the *htb1-G52D* and *htb1-P102L* mutants, we conducted an H2B^{ub}-ChIP experiment, which was validated in our previous study (Qin et al. 2024). Consistently, H2B^{ub} levels were significantly enriched at the transcribed genes *act1+* and *aro1+* in WT compared with the *htb1-K119R* mutant, but not at the intergenic region *ars2004*, which is not transcribed and has few H2B^{ub} (Fig. S6A). H2B^{ub} levels were also reduced at *act1+* and *aro1+*, but not at *ars2004*, in the *htb1-G52D* and *htb1-P102L* compared with WT (Fig. S6A). Importantly, we found that H2B^{ub} levels are decreased at *aat1+*, *eng1+*, and *ppk1+* in the *htb1-G52D* and *htb1-P102L* mutants (Fig. 6A), supporting that H2B^{ub} regulates the expression of these genes.

Previous studies demonstrated that H2B^{ub} is associated with elongating RNA polymerase II (pol II) in *S. cerevisiae* and reduced gene expression in *htb1-K119R* mutant is correlated with a transcriptional elongation defect in *S. pombe* (Xiao et al. 2005, Tanny et al. 2007). To understand how H2B^{ub} regulates gene expression in *htb1-G52D/D67N/P102L*, we analyzed RNA pol II levels in the representative genes using a ChIP-qPCR assay. The results showed

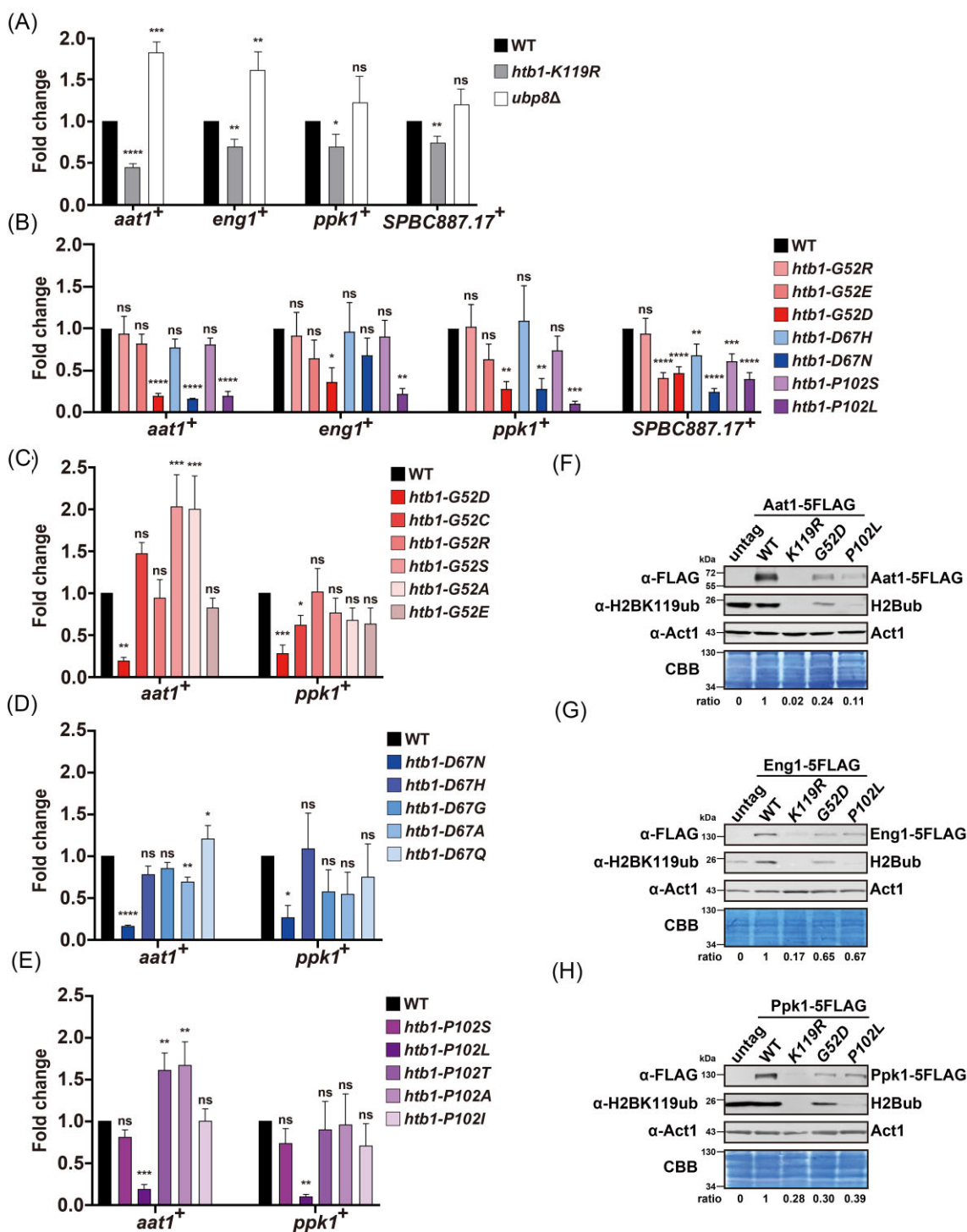


Figure 4. RT-qPCR and immunoblotting analysis of gene expression in the *htb1-Gly52/Asp67/Pro102* various mutants. (A) RT-qPCR analysis of *aat1*⁺, *eng1*⁺, *ppk1*⁺, and *SPBC887.17*⁺ transcripts in *htb1-K119R* (YGF226) and *ubp8Δ* (YGF415) mutants. (B) RT-qPCR validation of *aat1*⁺, *eng1*⁺, *ppk1*⁺, and *SPBC887.17*⁺ transcripts in the indicated and RNA-seq analyzed *htb1-Gly52/Asp67/Pro102* oncomutants. (C) RT-qPCR analysis of *aat1*⁺ and *ppk1*⁺ transcripts in *htb1-G52D* (YGF277), *htb1-G52C* (YGF507), *htb1-G52R* (YGF510), *htb1-G52S* (YGF460), *htb1-G52A* (YGF459), and *htb1-G52E* (YGF508) cells. (D) RT-qPCR analysis of *aat1*⁺ and *ppk1*⁺ transcripts in *htb1-D67N* (YGF324), *htb1-D67H* (YGF515), *htb1-D67G* (YGF514), *htb1-D67A* (YGF513), and *htb1-D67Q* (YGF509) cells. (E) RT-qPCR analysis of *aat1*⁺ and *ppk1*⁺ transcripts in *htb1-P102S* (YGF325), *htb1-P102L* (YGF279), *htb1-P102T* (YGF512), *htb1-P102A* (YGF511), and *htb1-P102I* (YGF505) cells. The fold change of gene expression in the indicated cells relative to that of WT (set as 1) is shown as mean ± SD (n = 3). A one-way analysis of variance (ANOVA) is performed to compare multiple data sets to WT. (F) Immunoblots of Aat1-5FLAG protein levels in untag (TK8), WT (YGF644), *htb1-K119R* (YGF645), *htb1-G52D* (YGF646), and *htb1-P102L* (YGF647) cells. (G) Immunoblots of Eng1-5FLAG protein levels in untag (TK8), WT (YGF632), *htb1-K119R* (YGF633), *htb1-G52D* (YGF634), and *htb1-P102L* (YGF635) cells. (H) Immunoblots of Ppk1-5FLAG protein levels in untag (TK8), WT (YGF591), *htb1-K119R* (YGF592), *htb1-G52D* (YGF594), and *htb1-P102L* (YGF595) cells. The intensity of the FLAG-tagged protein band is normalized to that of CBB staining. The fold change of this normalization factor in the indicated mutants relative to WT (set as 1) is depicted as the ratio at the bottom.

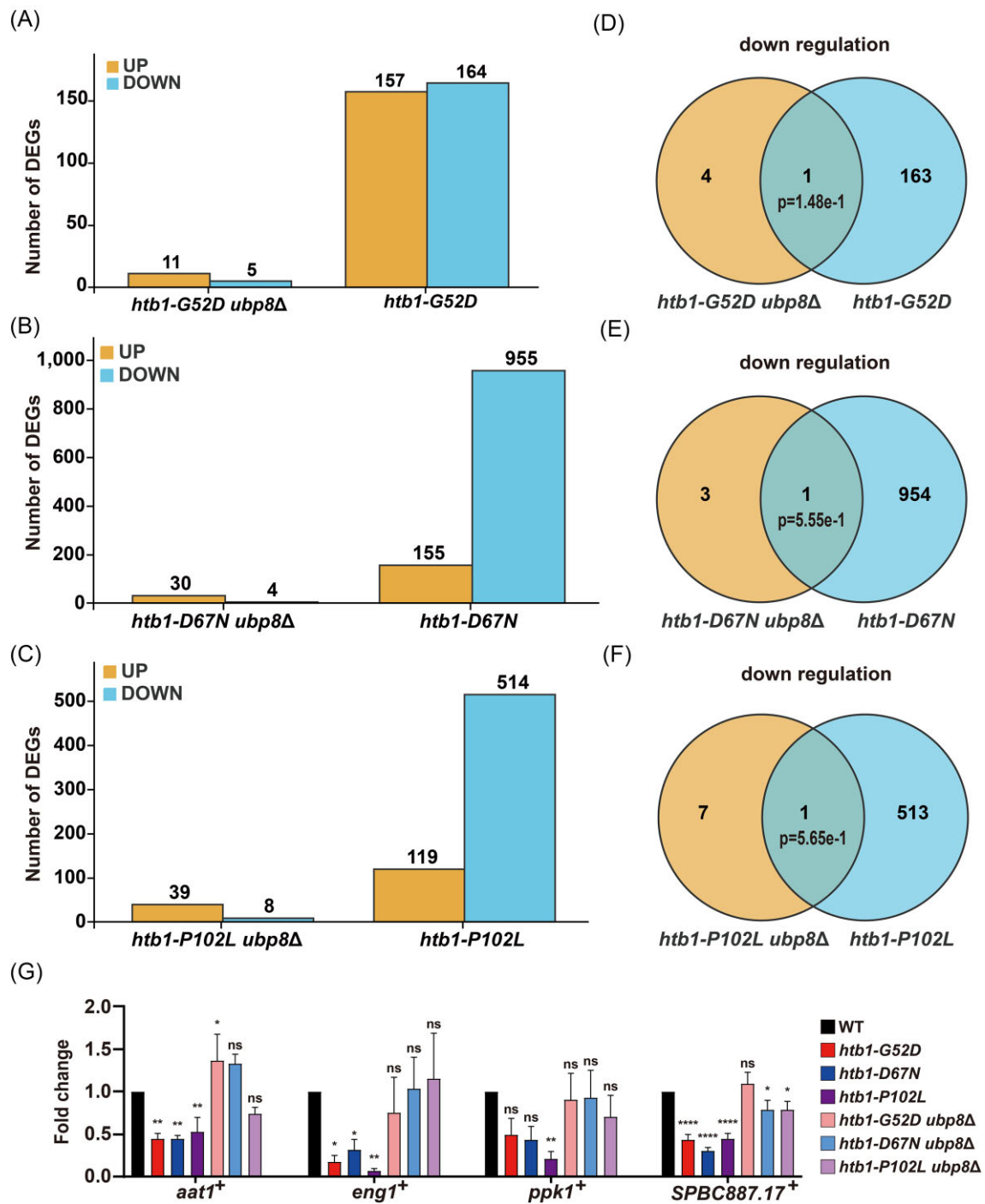


Figure 5. RNA-seq and RT-qPCR analysis of gene expression in the *htb1-G52D/D67N/P102L* oncomutants with *ubp8Δ*. (A) RNA-seq analysis of DEGs relative to WT cells in *htb1-G52D* (YGF277) and *htb1-G52D ubp8Δ* (YGF416) cells. (B) RNA-seq analysis of DEGs relative to WT cells in *htb1-D67N* (YGF324) and *htb1-D67N ubp8Δ* (YGF443) cells. (C) RNA-seq analysis of DEGs relative to WT cells in *htb1-P102L* (YGF279) and *htb1-P102L ubp8Δ* (YGF417) cells. The number of genes with up- and downregulated expression is indicated at the top of the column. (D) Venn Diagrams of downregulated genes in *htb1-G52D* (YGF277) and *htb1-G52D ubp8Δ* (YGF416). (E) Venn Diagrams of downregulated genes in *htb1-D67N* (YGF324) and *htb1-D67N ubp8Δ* (YGF443). (F) Venn Diagrams of downregulated genes in *htb1-P102L* (YGF279) and *htb1-P102L ubp8Δ* (YGF417). Fisher's exact test is used to calculate the P-values of significant differences in Venn Diagrams. (G) RT-qPCR of *aat1+*, *eng1+*, *ppk1+*, and *SPBC887.17+* transcripts in the *htb1-G52D*, *htb1-D67N*, and *htb1-P102L* oncomutants and their double mutants with *ubp8Δ*. The fold change of gene expression in the indicated cells relative to that of WT (set as 1) is shown as mean \pm SD ($n = 3$). A one-way ANOVA is performed for multiple comparisons to WT.

that RNA pol II levels at *aat1+*, *eng1+*, and *SPBC887.17+* were significantly reduced in *htb1-K119R*, *htb1-G52D*, *htb1-D67N*, and *htb1-P102L* compared with WT (Fig. 6B). However, RNA pol II levels were unaltered at *act1+* and *aro1+* (Fig. S6B), whose expression is

not regulated by H2B^{ub}. Collectively, these data further indicate that the compromised H2B^{ub} downregulates gene expression in *htb1-G52D*, *htb1-D67N*, and *htb1-P102L* by perturbing RNA pol II elongation.

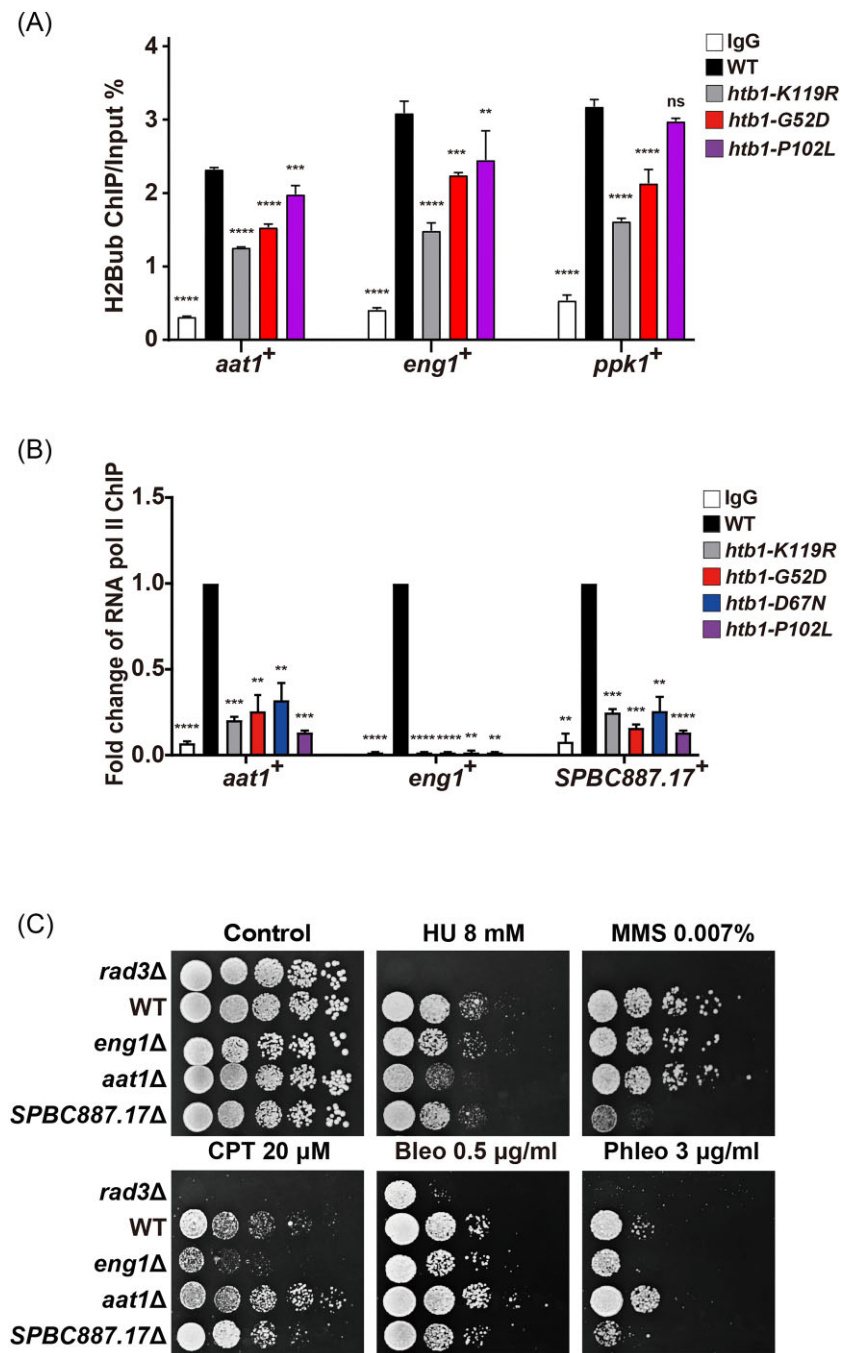


Figure 6. The ChIP-qPCR analysis of enrichment levels of H2B^{ub} and RNA pol II at the indicated genes in the *htb1-G52D/D67N/P102L* oncomutants, as well as the genotoxic phenotypes of those genes' deletion mutants. (A) The enrichment percentage of H2B^{ub} at *aat1*⁺, *eng1*⁺, and *ppk1*⁺ genes is shown in *htb1-K119R* (YGF226), *htb1-G52D* (YGF277), and *htb1-P102L* (YGF279). (B) The RNA pol II subunit Rpb1 enrichment at *aat1*⁺, *eng1*⁺, and *SPBC887.17*⁺ genes in *htb1-K119R* (YGF226), *htb1-G52D* (YGF277), *htb1-D67N* (YGF324), and *htb1-P102L* (YGF279) is relative to that in WT (TK8) (set as 1). The H2B^{ub} enrichment or relative fold change of RNA pol II levels is plotted as mean \pm SD ($n = 3$). A one-way ANOVA is performed for multiple comparisons to WT. (C) The genotoxic phenotypes of the *eng1Δ* (YGF651), *aat1Δ* (YGF652), and *SPBC887.17Δ* (YGF653) mutants. The length of incubation time is 4 days.

The deletion of *aat1*⁺, *eng1*⁺, and *SPBC887.17*⁺ leads to genotoxic defects and their overexpression partially suppresses the temperature sensitivity of *htb1-G52D*

Previous large-scale studies have suggested that the *ppk1Δ* mutant is sensitive to HU and thiabendazole, which interferes with microtubule polymerization (Bimbó et al. 2005, Pan et al. 2012), and that *eng1Δ* is sensitive to MMS and bleomycin (Rodríguez-López et al. 2023). To substantiate this, we constructed *eng1Δ*,

aat1Δ, and *SPBC887.17Δ* mutants and found that each was sensitive to at least one genotoxin (Fig. 6C). The *eng1Δ* exhibited sensitivities to CPT, bleomycin, and phleomycin. The *aat1Δ* showed the HU sensitivity. The *SPBC887.17Δ* was sensitive to MMS, bleomycin, and phleomycin (Fig. 6C). These data may partially explain why *htb1-G52D/D67N/P102L* with reduced levels of Aat1, Eng1, Ppk1, and *SPBC887.17* exhibit genotoxic sensitivity.

To determine whether the reduced expression of a particular gene is sufficient for the genotoxic defect of *htb1-G52D* and

htb1-P102L, we individually overexpressed *aat1*⁺, *eng1*⁺, *ppk1*⁺, and *SPBC887.17*⁺ from the moderate-strength *adh21* promoter in the *htb1*-G52D mutant. However, they failed to rescue the temperature and genotoxic sensitivities of *htb1*-G52D (Fig. S7A). To rule out the possibility that the relatively weak overexpression of Ppk1 was insufficient to compensate for the defective phenotypes of *htb1*-G52D, we additionally overexpressed *ppk1*⁺ from the strong-strength *adh11* promoter in WT, *htb1*-G52D, and *htb1*-P102L cells, but still observed no rescue effect (Fig. S7B). Furthermore, we overexpressed both *ppk1*⁺ and *aat1*⁺ from the *adh11* promoter and found that it partially rescued the temperature sensitivity of *htb1*-G52D but had no effect on genotoxic sensitivity (Fig. S7C). These data suggest that a set of altered transcripts controlled by H2B^{ub} may be required to contribute to the genomic instability of *htb1*-G52D, *htb1*-D67N, and *htb1*-P102L.

Discussion

We constructed diverse oncomutants of *htb1*-Gly52/Asp67/Pro102 in *S. pombe* and characterized their genotoxin susceptibility phenotypes, H2B^{ub} levels, and gene expression. Among them, only *htb1*-G52D, *htb1*-D67N, and *htb1*-P102L exhibit significant sensitivities to high temperature and genotoxins. Correlatively, the levels of H2B^{ub} are notably reduced only in the *htb1*-G52D, *htb1*-D67N, and *htb1*-P102L mutants. Mechanistically, the transcriptomes in *htb1*-G52D, *htb1*-D67N, and *htb1*-P102L cells are altered, which are overlapping with H2B^{ub}-regulated transcripts. These altered transcripts are largely restored to WT levels when H2B^{ub} levels are recovered in the absence of *ubp8*⁺. This coincides with the rescue of defective phenotypes in *htb1*-G52D, *htb1*-D67N, and *htb1*-P102L cells when H2B^{ub} levels are restored (Qin et al. 2024). Although we previously demonstrated that the compromised H2B^{ub} in *htb1*-G52D and *htb1*-P102L directly impairs Rad51 recruitment and causes HR repair defect, it does not generally affect the expression of DNA repair genes (Qin et al. 2024). Therefore, the alteration of genome-wide gene expression due to H2B^{ub} deficiency is a novel mechanism underlying the genomic instability of *htb1*-G52D, *htb1*-D67N, and *htb1*-P102L oncomutants. Collectively, we propose a model in which both HR repair and gene expression are two parallel and independent subpathways under the control of H2B^{ub}, whose deficiency plays a determining role in the genomic instability caused by H2B^{G52D}, H2B^{D67N}, and H2B^{P102L} oncohistones (Fig. 7).

The *htb1*-G52D/D67N/P102L mutants are similar to the *htb1*-G52E/D67Q/P102I mutants in producing amino acid changes with comparable characteristics, but these have not been reported as oncohistones and exhibit mild or no genotoxic defects and almost normal H2B^{ub} levels. In another aspect, nononcohistone *htb1*-D67A/P102A mutants also behave like WT. Therefore, our mutation spectra analyses indicate that only specific amino acid changes among the *htb1*-Gly52/Asp67/Pro102 diverse oncomutants, such as *htb1*-G52D, *htb1*-D67N, and *htb1*-P102L, have an impact on H2B^{ub} levels. The underlying reason is unclear. We previously indicated that the recruitment of Ubp8 onto the nucleosome is enhanced in the *htb1*-G52D mutant (Qin et al. 2024). Thus, we speculate that only the H2B^{G52D/D67N/P102L} changes can specifically remodel the nucleosome structure and promote the interaction of Ubp8 with the H2B in the nucleosome. To support this speculation, we predicted the nucleosome structures harboring diverse H2B-Gly52/Asp67/Pro102 changes. The negative charge of the H2B^{G52D} is supposed to weaken the H2B-DNA interaction with increased distance (Fig. S8A), which could destabilize the nucleosome and enhance nucleosome remodeling/sliding (Bagert et al.

2021, Jain and Strahl 2021). H2B^{D67N} is predicted to affect the contact with H4-Tyr98 on the histone dimer-tetramer interface (Fig. S8B), which may perturb histone exchange (Bagert et al. 2021, Jain and Strahl 2021). H2B^{P102L} could attenuate the hydrophobic interaction with H2A-Glu93/Lys96/Leu97 (Fig. S8C). However, the other H2B-Gly52/Asp67/Pro102 changes appear to have no such effects (Fig. S8A-C). The relevant structures need to be experimentally solved to test these predictions in the future.

This study revealed that the effects of different amino acid substitutions in oncohistone H2B on histone PTMs are generally associated with their oncogenic phenotypes such as genomic instability, which is consistent with the characteristic of oncohistone H3. Certain *htb1*-Gly52 oncomutants do not affect H2B^{ub} levels, yet they still exhibit genotoxic sensitivity. However, this is not found in *htb1*-Asp67/Pro102 oncomutants, where only the *htb1*-D67N and *htb1*-P102L affecting H2B^{ub} are defective in response to genotoxins. Our previous study on the synergistic genotoxic sensitivity of *htb1*-G52D K119R double mutant suggests that H2B^{G52D} not only reduces H2B^{ub} levels but also alters nucleosome remodeling independent of H2B^{ub}. However, the lack of synergistic sensitivity between *htb1*-D67N/P102L and *htb1*-K119R suggests that H2B^{D67N/P102L} primarily affect H2B^{ub} levels (Qin et al. 2024). Therefore, we propose that certain *htb1*-Gly52 mutants but not *htb1*-Asp67/Pro102 mutants could display genotoxic sensitivity by affecting nucleosome remodeling (Mitchener and Muir 2022), which is independent of H2B^{ub} regulation. This phenomenon is consistent with studies on H3 oncohistones in which the alteration of H3 PTMs is also not the sole mechanism for their phenotypes (Caeiro et al. 2024).

With respect to the relationship between histone PTMs and gene expression, the reduction in H3K27 and H3K36 methylation levels could not be mainly responsible for the changed gene expression in H3K27M, H3G34R/W, and H3K36M oncomutants. However, the reduction in H2B^{ub} seems to be the main cause of altered gene expression in *htb1*-G52D, *htb1*-D67N, and *htb1*-P102L. Thus, the impacts of altered histone PTMs on gene expression may be different in diverse histone oncomutants, which encourages us to study more noncanonical oncohistones in the future.

The mechanism by which dysregulated gene expression contributes to the genomic instability in *htb1*-G52D/D67N/P102L is still unclear. The individual overexpression of *aat1*⁺, *ppk1*⁺, *eng1*⁺, and *SPBC887.17*⁺ fails to compensate for the temperature and genotoxic defects of *htb1*-G52D. Interestingly, the combined overexpression of *aat1*⁺ and *ppk1*⁺ rescues the temperature sensitivity of *htb1*-G52D. Thus, the dysregulation of a particular transcript or protein could not be sufficient to contribute to genomic instability. Instead, we speculate that aberrant expression of a set of genes, which are regulated by H2B^{ub}, may play a synergistic role in the genomic instability of *htb1*-G52D/D67N/P102L. Furthermore, a previous study suggested that altered expression of significantly clustered genes controlled by H2B^{ub} plays a specific role in the stress response (Tanny et al. 2007); thus, it is also possible that H2B^{ub}-mediated alterations of gene expression in *htb1*-G52D/D67N/P102L impair the response to DNA replication and damage stress.

Two genetic approaches are used in yeast to model oncohistones in cancer (Zhang et al. 2023). A single allele of a histone gene can be introduced with oncomutations and the other alleles are kept intact or deleted, which express oncohistone mutants either in the presence or the absence of WT histone proteins. The yeast cells expressing the oncohistone within many WT histone proteins closely model cancer cells, where only one copy of many histone genes is mutated, and allow analysis of dominant-negative effects and phenotypes. Alternatively, the yeast cells expressing

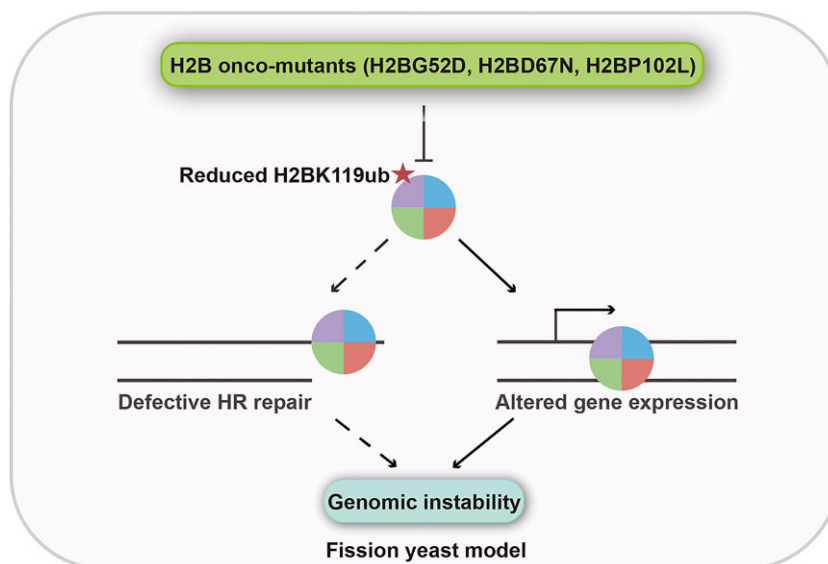


Figure 7. A unified model is proposed. The diverse oncomutants at H2B-Gly52/Asp67/Pro102 residues are modeled and characterized in the fission yeast *S. pombe*. Only the H2BG52D, H2BD67N, and H2BP102L exhibit significant genomic instability. Mechanistically, the compromised H2B^{ub} in H2BG52D/D67N/P102L plays a crucial role. It not only impairs the HR repair efficiency but also alters the genome-wide gene expression. The diagrams with dashed lines represent our previous findings (Qin et al. 2024), and those with solid lines represent the findings in this study.

the oncohistone as the sole copy of the histone protein provide direct and clean characterization of oncohistone function as well as rapid and unbiased screening for recessive phenotypes (Zhang et al. 2023). In this study, oncomutations that occur in the sole H2B gene *htb1*⁺ in *S. pombe* cells amplify their effects in the absence of WT H2B protein, which provides an advantage for detecting even small impacts of H2B oncohistones. In our previous study, H2B^{G52D/P102L} in the presence of WT H2B protein also lead to genotoxic sensitivity and reduction in H2B^{ub} *in cis* (Qin et al. 2024), but the dominant-negative effect of reduced H2B^{ub} in local genes on their expression is still unclear and is under current investigation. In human cancers, only one of the many H2B gene copies is mutated. The effects of H2B^{G52D/D67N/P102L} on gene expression, if there is any effect, could be confined to a few genes with the incorporation of an H2B oncohistone. It is also unclear whether these limited alterations in gene expression contribute to genomic instability and oncogenesis. Thus, whether the findings in this study can be applied to human cancer cells needs to be investigated in the future.

Conclusion

In summary, we extended our previous study on H2B oncohistones in *S. pombe* and revealed that the specific amino acid substitutions in *htb1*-Gly52/Asp67/Pro102 oncomutants, such as *htb1*-G52D, *htb1*-D67N, and *htb1*-P102L, cause genotoxic sensitivity and genomic instability. The underlying mechanisms include defective HR repair and altered gene expression, both of which are caused by the reduction in H2B^{ub} levels. Therefore, H2B^{ub} levels reduced by H2B oncohistones play a key role in oncogenesis.

Acknowledgments

We thank Dr Ying Huang's laboratory (Nanjing Normal University) for support, Dr Quanwen Jin (Xiamen University) for providing plasmids, and Dr Yao Yu and Dr Hong Lu (Fudan University) for providing strains.

Supplementary data

Supplementary data are available in the *FEMSYR* Journal online.

Conflict of interest: The authors have no conflicts of interests.

Funding

This work was supported by a grant (31900403 to G.F.) from the National Natural Science Foundation of China.

Data availability

The RNA-seq data have been deposited to Gene Expression Omnibus (GEO) under accession numbers GSE267247 and GSE290173. The other original data and resources are available from the corresponding author upon request.

References

- Abramson J, Adler J, Dunger J et al. Accurate structure prediction of biomolecular interactions with AlphaFold 3. *Nature* 2024;**630**:493–500. <https://doi.org/10.1038/s41586-024-07487-w>.
- Bagert JD, Mitchener MM, Patriotis AL et al. Oncohistone mutations enhance chromatin remodeling and alter cell fates. *Nat Chem Biol* 2021;**17**:403–11. <https://doi.org/10.1038/s41589-021-00738-1>.
- Bähler J, Wu JQ, Longtine MS et al. Heterologous modules for efficient and versatile PCR-based gene targeting in *Schizosaccharomyces pombe*. *Yeast* 1998;**14**:943–51. [https://doi.org/10.1002/\(SICI\)1097-0061\(199807\)14:10%3c943::AID-YEA292%3e3.0.CO;2-Y](https://doi.org/10.1002/(SICI)1097-0061(199807)14:10%3c943::AID-YEA292%3e3.0.CO;2-Y).
- Bennett RL, Bele A, Small EC et al. A mutation in histone H2B represents a new class of oncogenic driver. *Cancer Discov* 2019;**9**:1438–51. <https://doi.org/10.1158/2159-8290.CD-19-0393>.
- Bimbó A, Jia Y, Poh SL et al. Systematic deletion analysis of fission yeast protein kinases. *Eukaryot Cell* 2005;**4**:799–813. <https://doi.org/10.1128/EC.4.4.799-813.2005>.
- Caeiro LD, Verdun RE, Morey L. Histone H3 mutations and their impact on genome stability maintenance. *Biochem Soc Trans* 2024;**52**:2179–91. <https://doi.org/10.1042/BST20240177>.

- Chan KM, Fang D, Gan H et al. The histone H3.3K27M mutation in pediatric glioma reprograms H3K27 methylation and gene expression. *Genes Dev* 2013;**27**:985–90. <https://doi.org/10.1101/gad.217778.113>.
- Chen JJ, Stermer D, Tanny JC. Decoding histone ubiquitylation. *Front Cell Dev Biol* 2022;**10**:968398. <https://doi.org/10.3389/fcell.2022.968398>.
- Dabin J, Giacomini G, Petit E et al. New facets in the chromatin-based regulation of genome maintenance. *DNA Repair* 2024;**140**:103702. <https://doi.org/10.1016/j.dnarep.2024.103702>.
- D'Aquino KE, Monje-Casas F, Paulson J et al. The protein kinase Kin4 inhibits exit from mitosis in response to spindle position defects. *Mol Cell* 2005;**19**:223–34. <https://doi.org/10.1016/j.molcel.2005.06.005>.
- Ekal L, Alqahtani AMS, Schuldiner M et al. Spindle position checkpoint kinase Kin4 regulates organelle transport in *Saccharomyces cerevisiae*. *Biomolecules* 2023;**13**:1098. <https://doi.org/10.3390/biom13071098>.
- Espinoza Pereira KN, Shan J, Licht JD et al. Histone mutations in cancer. *Biochem Soc Trans* 2023;**51**:1749–63. <https://doi.org/10.1042/BS20210567>.
- Fang J, Huang Y, Mao G et al. Cancer-driving H3G34V/R/D mutations block H3K36 methylation and H3K36me3-MutS α interaction. *Proc Natl Acad Sci USA* 2018;**115**:9598–603. <https://doi.org/10.1073/pnas.1806355115>.
- Feng G, Leem YE, Levin HL. Transposon integration enhances expression of stress response genes. *Nucleic Acids Res* 2013;**41**:775–89. <https://doi.org/10.1093/nar/gks1185>.
- Feng G, Yuan Y, Li Z et al. Replication fork stalling elicits chromatin compaction for the stability of stalling replication forks. *Proc Natl Acad Sci USA* 2019;**116**:14563–72. <https://doi.org/10.1073/pnas.1821475116>.
- Forsburg SL, Rhind N. Basic methods for fission yeast. *Yeast* 2006;**23**:173–83. <https://doi.org/10.1002/yea.1347>.
- Fuchs G, Oren M. Writing and reading H2B monoubiquitylation. *Biochim Biophys Acta Gene Regul Mech* 2014;**1839**:694–701. <https://doi.org/10.1016/j.bbagr.2014.01.002>.
- Funato K, Tabar V. Histone mutations in cancer. *Annu Rev Cancer Biol* 2018;**2**:337–51. <https://doi.org/10.1146/annurev-cancerbio-030617-050143>.
- Jain K, Strahl BD. Oncohistones: corruption at the core. *Nat Chem Biol* 2021;**17**:370–1. <https://doi.org/10.1038/s41589-021-00764-z>.
- Jain SU, Khazaei S, Marchione DM et al. Histone H3.3 G34 mutations promote aberrant PRC2 activity and drive tumor progression. *Proc Natl Acad Sci USA* 2020;**117**:27354–64. <https://doi.org/10.1073/pnas.2006076117>.
- Jumper J, Evans R, Pritzel A et al. Highly accurate protein structure prediction with AlphaFold. *Nature* 2021;**596**:583–9. <https://doi.org/10.1038/s41586-021-03819-2>.
- Kallappagoudar S, Yadav RK, Lowe BR et al. Histone H3 mutations—a special role for H3.3 in tumorigenesis?. *Chromosoma* 2015;**124**:177–89. <https://doi.org/10.1007/s00412-015-0510-4>.
- Lemon LD, Kannan S, Mo KW et al. A *Saccharomyces cerevisiae* model and screen to define the functional consequences of oncogenic histone missense mutations. *G3* 2022;**12**. <https://doi.org/10.1093/g3journal/jkac120>.
- Leng AM, Radmall KS, Shukla PK et al. Quantitative assessment of histone H2B monoubiquitination in yeast using immunoblotting. *MPS* 2022;**5**:74. <https://doi.org/10.3390/mps5050074>.
- Lewis PW, Müller MM, Koletsky MS et al. Inhibition of PRC2 activity by a gain-of-function H3 mutation found in pediatric glioblastoma. *Science* 2013;**340**:857–61. <https://doi.org/10.1126/science.1232245>.
- Liu X, McEachron TA, Schwartzentruber J et al. Histone H3 mutations in pediatric brain tumors. *Cold Spring Harb Perspect Biol* 2014;**6**:a018689. <https://doi.org/10.1101/cshperspect.a018689>.
- Lowe BR, Maxham LA, Hamey JJ et al. Histone H3 mutations: an updated view of their role in chromatin deregulation and cancer. *Cancers* 2019;**11**:1–24. <https://doi.org/10.3390/cancers11050660>.
- Lowe BR, Yadav RK, Henry RA et al. Surprising phenotypic diversity of cancer-associated mutations of Gly 34 in the histone H3 tail. *eLife* 2021;**10**:1–30. <https://doi.org/10.7554/eLife.65369>.
- Lu C, Jain SU, Hoelper D et al. Histone H3K36 mutations promote sarcomagenesis through altered histone methylation landscape. *Science* 2016;**352**:844–9. <https://doi.org/10.1126/science.aac7272>.
- Lu G, Tang Z, Wu M et al. SRPKs homolog Dsk1 regulates homologous recombination repair in *Schizosaccharomyces pombe*. *Genes Cells* 2025;**30**:e13192. <https://doi.org/10.1111/gtc.13192>.
- Mitchener MM, Muir TW. Oncohistones: exposing the nuances and vulnerabilities of epigenetic regulation. *Mol Cell* 2022;**82**:2925–38. <https://doi.org/10.1016/j.molcel.2022.07.008>.
- Mohammad F, Helin K. Oncohistones: drivers of pediatric cancers. *Genes Dev* 2017;**31**:2313–24. <https://doi.org/10.1101/gad.309013.117>.
- Nacev BA, Feng L, Bagert JD et al. The expanding landscape of 'oncohistone' mutations in human cancers. *Nature* 2019;**567**:473–8. <https://doi.org/10.1038/s41586-019-1038-1>.
- Ohkuni K, Au W-C, Kazi AZ et al. Oncohistone H3 E97K mutation facilitates CENP-A mislocalization and chromosomal instability in budding yeast. *Nucleic Acids Res* 2025;**53**. <https://doi.org/10.1093/nar/gkaf083>.
- Pan X, Lei B, Zhou N et al. Identification of novel genes involved in DNA damage response by screening a genome-wide *Schizosaccharomyces pombe* deletion library. *BMC Genomics* 2012;**13**:662. <https://doi.org/10.1186/1471-2164-13-662>.
- Pereira G, Schiebel E. Kin4 kinase delays mitotic exit in response to spindle alignment defects. *Mol Cell* 2005;**19**:209–21. <https://doi.org/10.1016/j.molcel.2005.05.030>.
- Qin B, Lu G, Chen X et al. H2B oncohistones cause homologous recombination defect and genomic instability through reducing H2B monoubiquitination in *Schizosaccharomyces pombe*. *J Biol Chem* 2024;**300**:107345. <https://doi.org/10.1016/j.jbc.2024.107345>.
- Qiu L, Hu X, Jing Q et al. Mechanism of cancer: oncohistones in action. *J Genet Genomics* 2018;**45**:227–36. <https://doi.org/10.1016/j.jgg.2018.04.004>.
- Rodríguez-López M, Bordin N, Lees J et al. Broad functional profiling of fission yeast proteins using phenomics and machine learning. *eLife* 2023;**12**. <https://doi.org/10.7554/eLife.88229>.
- Sabatinos SA, Forsburg SL. Molecular genetics of *Schizosaccharomyces pombe*. *Methods Enzymol* 2010;**470**:759–95. [https://doi.org/10.1016/S0076-6879\(10\)70032-X](https://doi.org/10.1016/S0076-6879(10)70032-X).
- Sad K, Fawwal DV, Jones CY et al. Histone H3E50K remodels chromatin to confer oncogenic activity and support an EMT phenotype. *NAR Cancer* 2025;**7**. <https://doi.org/10.1093/narcan/zcaf002>.
- Sahu V, Lu C. Oncohistones: hijacking the histone code. *Annu Rev Cancer Biol* 2022;**6**:293–312. <https://doi.org/10.1146/annurev-cancerbio-070120-102521>.
- Selvam K, Wyrick JJ, Parra MA. DNA repair in nucleosomes: insights from histone modifications and mutants. *Int J Mol Sci* 2024;**25**:4393. <https://doi.org/10.3390/ijms25084393>.
- Shan C-M, Wang J, Xu K et al. A histone H3K9M mutation traps histone methyltransferase Clr4 to prevent heterochromatin spreading. *eLife* 2016;**5**:1–18. <https://doi.org/10.7554/eLife.17903>.

- Shi L, Shi J, Shi X et al. Histone H3.3 G34 mutations alter histone H3K36 and H3K27 methylation in cis. *J Mol Biol* 2018;**430**:1562–5. <https://doi.org/10.1016/j.jmb.2018.04.014>.
- Tanny JC, Erdjument-Bromage H, Tempst P et al. Ubiquitylation of histone H2B controls RNA polymerase II transcription elongation independently of histone H3 methylation. *Genes Dev* 2007;**21**:835–47. <https://doi.org/10.1101/gad.1516207>.
- Tessadori F, Giltay JC, Hurst JA et al. Germline mutations affecting the histone H4 core cause a developmental syndrome by altering DNA damage response and cell cycle control. *Nat Genet* 2017;**49**:1642–6. <https://doi.org/10.1038/ng.3956>.
- Wan YCE, Chan KM. Histone H2B mutations in cancer. *Biomedicines* 2021;**9**:694. <https://doi.org/10.3390/biomedicines9060694>.
- Wan YCE, Liu J, Chan KM. Histone H3 mutations in cancer. *Curr Pharmacol Rep* 2018;**4**:292–300. <https://doi.org/10.1007/s40495-018-0141-6>.
- Weinberg DN, Allis CD, Lu C. Oncogenic mechanisms of histone H3 mutations. *Cold Spring Harb Perspect Med* 2017;**7**:a026443. <https://doi.org/10.1101/cshperspect.a026443>.
- Xiao T, Kao C-F, Krogan NJ et al. Histone H2B ubiquitylation is associated with elongating RNA polymerase II. *Mol Cell Biol* 2005;**25**:637–51. <https://doi.org/10.1128/MCB.25.2.637-651.2005>.
- Yadav P, Jain R, Yadav RK. Emerging roles of cancer-associated histone mutations in genomic instabilities. *Front Cell Dev Biol* 2024;**12**. <https://doi.org/10.3389/fcell.2024.1455572>.
- Yadav RK, Jablonowski CM, Fernandez AG et al. Histone H3G34R mutation causes replication stress, homologous recombination defects and genomic instability in *S. pombe*. *eLife* 2017;**6**:1–28. <https://doi.org/10.7554/eLife.27406>.
- Zhang X, Fawwal DV, Spangle JM et al. Exploring the molecular underpinnings of cancer-causing oncohistone mutants using yeast as a model. *J Fungi* 2023;**9**:1187. <https://doi.org/10.3390/jof9121187>.